Durable SiO2-ZrO2-Ag coatings produced via co-sputtering method for sustained antimicrobial activity on air filtration media

Surface & Coatings Technology 536 (2026) 133757

Contents lists available at ScienceDirect

Surface & Coatings Technology

journal homepage: www.elsevier.com/locate/surfcoat

Durable SiO_2-ZrO_2-Ag coatings produced via co-sputtering method for sustained antimicrobial activity on air filtration media

Angelica Luceri, Mariacristina Martorino, Francesco Baino, Cristina Balagna *

Institute of Materials Physics and Engineering, Department of Applied Science and Technology, Politecnico di Torino, Corso Duca degli Abruzzi 24, 10129, Torino, Italy

ARTICLE INFO

Keywords:
Antimicrobial coatings
Silver nanoclusters
PVD
HEPA filters
Bioaerosol

ABSTRACT

The development of multifunctional antimicrobial surfaces is critical for healthcare, air filtration, and hygiene-sensitive applications. In this work, innovative SiO_2–ZrO_2–Ag composite coatings were obtained via physical-vapor deposition (PVD) co-sputtering, and successfully applied on both cotton fabrics and high-efficiency particulate air (HEPA) H14 filters. The coatings consist of a robust silica–zirconia matrix embedding silver nanoclusters, providing simultaneous chemical stability, controlled silver release, and broad-spectrum antibacterial activity. Morphological, compositional, and structural analyses confirmed uniform deposition, amorphous matrix formation, and nanoscale silver cluster incorporation. Antibacterial performance was evaluated through inhibition halo assays, CFU counting, and a bioaerosol contamination test, demonstrating effective suppression of both Gram-positive (*Staphylococcus epidermidis*) and Gram-negative (*Escherichia coli*) bacteria, as well as reduced surface colonization under realistic conditions. Durability tests revealed sustained antibacterial efficacy after repeated washing cycles, highlighting the long-term stability of the coatings. Overall, the results suggest a versatile and potentially scalable strategy for producing antimicrobial surfaces with tunable properties, offering a promising solution for textiles, filtration systems, and other applications requiring long-lasting microbial control.

1. Introduction

Indoor air quality (IAQ) has become a major public health concern, as bioaerosol accumulation in relatively closed or confined environments significantly contributes to respiratory diseases and healthcare-associated infections (HAIs) [1–4]. Although heating, ventilation and air conditioning (HVAC) systems equipped with filtration units can remove airborne particulates [5], filters may also act as reservoirs for microbial growth [6] and re-aerosolization, thus increasing contamination risks if not properly maintained [7]. The necessity for active, long-term antimicrobial protection on air filtration media is thus paramount, as conventional disinfection methods often lack sustained efficacy and can introduce harmful residues [8,9]. Silver nanoparticles (AgNPs) are among the most effective broad-spectrum antimicrobial agents, acting through controlled Ag^+ release, ROS generation, and bacterial membrane disruption [10–12]. However, Ag-containing coatings obtained through traditional deposition routes can suffer from limited durability, weak mechanical adhesion and uncontrolled silver release [13]. Embedding AgNPs within a stable inorganic matrix is therefore essential to ensure sustained antibacterial performance. Silica (SiO_2) has been widely investigated for this purpose, due to its chemical stability, biocompatibility, and ability to host metal nanoclusters, while enabling gradual ion release [14–19]. Recent studies have shown that spherical silica particles functionalized with silver ions exhibit strong antimicrobial activity against antibiotic-resistant strains, too, making them promising candidates for frequently touched or contaminated surfaces [20]. Research on silver–silica systems has increasingly focused on tailoring morphology and enhancing antibacterial performance. For instance, *Fernandez-Lodeiro* et al. [21] employed adenosine monophosphate to obtain homogeneous silica shells around AgNPs, achieving controlled dissolution and significant activity against Gram-negative bacteria. Similarly, the surface charge and shell thickness of mesoporous silica-coated AgNPs embedded in polymers were shown to strongly affect bactericidal action toward *E. coli* and *S. aureus* [22]. In addition to structural and surface modifications, the development of hybrid silica-based systems has attracted increasing attention as a strategy to further tune antimicrobial activity and surface functionality. As demonstrated, for example, by chitosan-coated silica beads functionalized with AgNPs [23], or titania–silica xerogels that improve both hydrophilicity and antimicrobial resistance via sustainable synthesis

* Corresponding author.
E-mail address: cristina.balagna@polito.it (C. Balagna).

https://doi.org/10.1016/j.surfcoat.2026.133757
Received 18 March 2026; Received in revised form 11 June 2026; Accepted 9 July 2026
Available online 10 July 2026

[24]. Green synthesis approaches based on plant extracts have recently emerged as promising alternatives for the production of antibacterial and antiviral AgNPs. In particular, bioactive compounds derived from *Camellia chrysantha* and *Quisqualis indica* were shown to promote nanoparticle stabilization and enhance antimicrobial activity, demonstrating the potential of eco-friendly synthesis routes for biomedical applications [25,26].

Apart from silica coatings, zirconia-based materials have also attracted recent attention due to their antimicrobial potential and better long-term stability upon contact with aqueous media. For example, porous zirconia impregnated with silver nitrate enabled excellent nanoparticle dispersion and improved antibacterial response, making it suitable for implant applications [27]. Given the increasing need to control airborne microbial transmission, several antimicrobial filtration strategies have been proposed, including PLA/chitosan membranes [28], triclosan-modified PP filters, graphene–silver hybrids [29], chlorhexidine-treated fibers [30], AgNP-coated nanofibers [31,32], and multifunctional Ag/ZnO/TiO_2 nanocoatings [33]. However, many of these systems still face challenges related to durability, adhesion, and controlled silver release. Although silver coatings are widely recognized for their strong antibacterial activity, maintaining long-term performance requires controlling silver release and preventing rapid depletion of the active phase. Embedding silver nanoclusters within inorganic oxide matrices has therefore been widely investigated as a strategy to moderate Ag^+ release, improve coating durability, and prolong antimicrobial activity over time. Silica-based matrices, in particular, can promote gradual ion release, while zirconia contributes to enhanced chemical stability in aqueous environments [15,17]. In this context, the combination of SiO_2 and ZrO_2 is particularly attractive, since silica promotes controlled ion diffusion whereas zirconia improves chemical durability and resistance to hydrolytic degradation. Beyond antibacterial performance, this approach also supports the development of more durable and resource-efficient antimicrobial systems, in line with sustainability and circular-economy principles. In this context, durability should not be interpreted as filter recyclability or repeated regeneration, but rather as the ability of the antimicrobial coating to maintain functionality and structural integrity throughout the operational lifetime of the filtration material, while minimizing uncontrolled silver dispersion into the environment.

Unlike previously reported single-oxide systems (SiO_2 or ZrO_2), this work proposes a hybrid SiO_2–ZrO_2 matrix designed to decouple silver release and chemical stability. This dual-function approach enables a balance between sustained antibacterial activity and resistance to aqueous degradation, which may be difficult to achieve using single-oxide coatings. Although PVD primarily modifies the outermost fibers, microbial colonization is known to occur mainly on the exposed surface layers, making surface functionalization an effective strategy.

2. Materials and methods

2.1. Deposition of composite coatings

The PVD co-sputtering technique was employed for the deposition of composite coatings, leveraging the versatility of this method that enables the simultaneous use of multiple targets through a simple and environmentally friendly process. The coatings consisted of a mixed SiO_2 and ZrO_2 matrix (the latter selected due to its stability and durability) incorporating silver (Ag) nanoclusters to impart antibacterial functionality. The deposition was carried out following a patented procedure [34], with each target operating under specific power conditions optimised based on previous studies and tailored to the intended application. In particular, the silica target (99.99% SiO_2, Nanovision™) was powered at 200 W in radio frequency (RF) mode, the zirconia target (99.98% ZrO_2, Nanovision™) at 250 W in RF mode, and the silver target (99.9% Ag, Franco Corradi) at 5 W in direct current (DC) mode. The process was performed in a pure argon atmosphere at a pressure of 5.5 dPa for a total deposition time of 1 h. The coatings were deposited on commercial high-efficiency particulate air (HEPA) H14 filters, which can retain at least 99.97% of particles $\geq$0.3 μm, including dust and bacteria. The functionalization aimed at conferring antibacterial activity, thereby inhibiting bacterial proliferation on the filter surface. To further assess coating durability, including resistance to water exposure and washing cycles, additional depositions were carried out on commercial cotton fabrics, used as model substrates to evaluate coating stability under extreme aqueous exposure conditions, rather than to replicate real HEPA operating conditions [17,35].

2.2. Chemical, morphological and structural analyses

The chemical composition of the coatings was analysed by energy-dispersive spectroscopy (EDS, EDAX PV 9900™), determining the atomic percentages of Si, Zr, and Ag, while the surface morphology was investigated by field-emission scanning electron microscopy (FESEM, QUANTA INSPECT 200; Zeiss SUPRA 40). Additional nanoscale morphological and compositional analyses of the SiO_2–ZrO_2–Ag coatings were performed by high-resolution scanning transmission electron microscopy (HR-STEM, Talos Thermo Scientific, LaB_6 source) operated at 200 kV. The acquired HR-STEM images were subsequently processed and analysed using ImageJ software. Structural analysis was performed by X-ray diffraction (XRD, Bragg–Brentano X'Pert, Philips) in grazing incidence mode, using a fixed incidence angle of 1°, to assess the amorphous or crystalline nature of the SiO_2–ZrO_2 matrix and to detect the presence of Ag nanoclusters. Complementary optical characterization was carried out by UV–Visible absorption spectroscopy (UV–Vis, Shimadzu UV-2600) in the 200–700 nm range to further support the formation of silver nanoclusters.

2.3. Silver ion release test

The release of Ag ions from the composite coatings was assessed by ion release experiments in aqueous medium. Specifically, coated cotton specimens (1 × 1 cm^2) were immersed in 30 mL of Milli-Q water at room temperature, with the functionalized surface oriented upward. The release medium was collected after 1 h, 3 h, and 1, 7, and 14 days. For each time point, three replicate samples were analysed in duplicate. The concentration of silver ions released into the solution (ppm) was quantified using a Hanna Instruments™ spectrophotometer. Silver concentration was expressed as mean ± standard deviation.

2.4. Antibacterial tests

2.4.1. Inhibition halo test

The inhibition halo test was employed to qualitatively assess the antibacterial activity of Ag-containing coatings, following the NCCLS M2-A9 protocol [36]. The assay measures bacterial growth suppression through the formation of inhibition zones surrounding coated samples placed on inoculated agar plates. Tests were conducted on SiO_2–ZrO_2 and SiO_2–ZrO_2–Ag coated cotton fabrics, as well as on SiO_2–ZrO_2–Ag coated HEPA filters. Uncoated substrates were used as negative controls. Two bacterial strains were selected: the Gram-positive *Staphylococcus epidermidis* (ATCC 14990) and the Gram-negative *Escherichia coli* (ATCC 8739). Bacteria were initially cultured on Columbia Blood Agar (*S. epidermidis*) and Nutrient Agar (*E. coli*), then suspended in Mueller–Hinton broth and adjusted to 0.5 McFarland turbidity standard (≈10^8 CFU/mL). The suspensions were spread on Nutrient Agar plates, and coated square samples (10 mm × 10 mm) were placed on the agar surface with the coated side facing downward. After incubation at 35 °C for 24 h, the diameters of inhibition zones were measured to assess antibacterial performance. Results were expressed as mean ± standard deviation. In the presence of multiple (concentric) inhibition zones, the outer antibacterial halo was considered for quantitative analysis.

2.4.2. Durability of antibacterial coatings under repeated washing

The washing resistance test was designed to evaluate both the chemical durability of the coatings in aqueous environments and the preservation of antibacterial functionality upon repeated washing. Cotton was used as a model substrate to simulate extreme aqueous exposure conditions and evaluate coating stability, rather than to replicate real HEPA operating conditions. Washing durability was assessed in terms of both coating retention and preservation of antibacterial activity. For each cycle, fabric specimens (20 mm × 20 mm) were immersed in 100 mL of Milli-Q water containing 0.2 g of standardized detergent (WOB 1993, Testfabrics Inc.), and agitated in a thermostatic bath at 50 °C and 130 rpm for 30 min. The samples were then rinsed with distilled water and air-dried at room temperature before characterization. Tests were performed after 5, 10, and 20 cycles. Post-washed samples were analysed by EDS to determine elemental retention and by inhibition halo assays to confirm antibacterial efficacy.

2.4.3. Count of the colonies forming units (CFU) test

Quantitative antibacterial efficacy was determined by CFU counting according to the NCCLS M7-A6 protocol [37]. The assay was carried out on uncoated filters, SiO_2–ZrO_2–Ag coated filters (20 mm × 5 mm), and broth-only controls, using *Staphylococcus epidermidis* as the test strain. Bacterial suspensions (5×10^5 CFU/mL) were prepared in Mueller–Hinton broth, and the samples were immersed in the medium. After incubation at 35 °C for 24 h, two complementary analyses were performed: (i) bacterial proliferation in broth – the culture medium in which the samples were incubated was collected and subjected to CFU counting to evaluate the extent of bacterial growth in the surrounding environment, and (ii) bacterial adhesion to the filter surface – after incubation, the filters were transferred into sterile saline and treated by vortexing followed by ultrasonication to detach microorganisms adhered to the surface. The resulting suspensions were serially diluted, and 100 µL aliquots were plated on Columbia Blood Agar and incubated for 24 h at 35 °C. Colony counts were converted into CFU values according to the equation:

$$CFU = number\ of\ colonies \times dilution\ factor$$

2.4.4. Contamination test

To simulate realistic operating conditions, a bioaerosol contamination test was performed on HEPA filters, according to the method described in the CEN Workshop Agreement CWA 18309:2025 [38]. *Staphylococcus epidermidis* was selected as the model bacterium, while uncoated filters served as controls. A concentrated bacterial broth was prepared by incubating *S. epidermidis* in brain heart infusion (BHI) medium for 24 h, reaching a McFarland index of ≈7. This suspension was aerosolized using a bioaerosol generator (TOPAS ATM 220) and directed through a funnel onto coated and uncoated filter samples (40 mm × 40 mm for qualitative analysis, 20 mm × 5 mm for quantitative assessment) (Fig. 1). Following a 30 min exposure, two complementary evaluations were performed. To have a qualitative assessment, exposed filters were placed onto Mueller–Hinton agar plates and incubated for 24 h at 35 °C. The presence or absence of colonies on the contact agar surface was used to visually assess antibacterial efficacy. For the quantitative assessment, the exposed filters were immersed in sterile Mueller–Hinton broth (free of bacteria) and incubated for 24 h at 35 °C. Bacterial proliferation in the broth was evaluated by CFU counting, as described in Section 2.4.3. In parallel, the same filters were vortexed and ultrasonicated in saline to detach adhered bacteria, allowing quantification of bacterial colonization directly on the filter surface. This approach enabled the evaluation of both airborne contamination resistance and surface colonization under conditions mimicking real filter operation.

3. Results and discussion

3.1. Morphological, chemical and structural analysis

Images of cotton fabrics and HEPA H14 filter are reported in Fig. 2. In particular, the uncoated cotton substrate (Fig. 2(a)) and the uncoated HEPA filter (Fig. 2(d)), at low magnifications, showed a smooth and randomly distributed fibrous network.

At high magnification, FESEM uncoated cotton and HEPA (Fig. 2(b) and (e)) displayed smooth surfaces, while the SiO_2–ZrO_2–Ag coated fibers (Fig. 2(c) and (f)) exhibited a homogeneous layer with globular morphology, confirming successful deposition. The coating appeared continuous and evenly distributed along the fiber surfaces. At this magnification, silver nanoclusters, which are embedded within the silica–zirconia matrix, are not individually distinguishable.

To further investigate the nanoscale morphology of the coating and

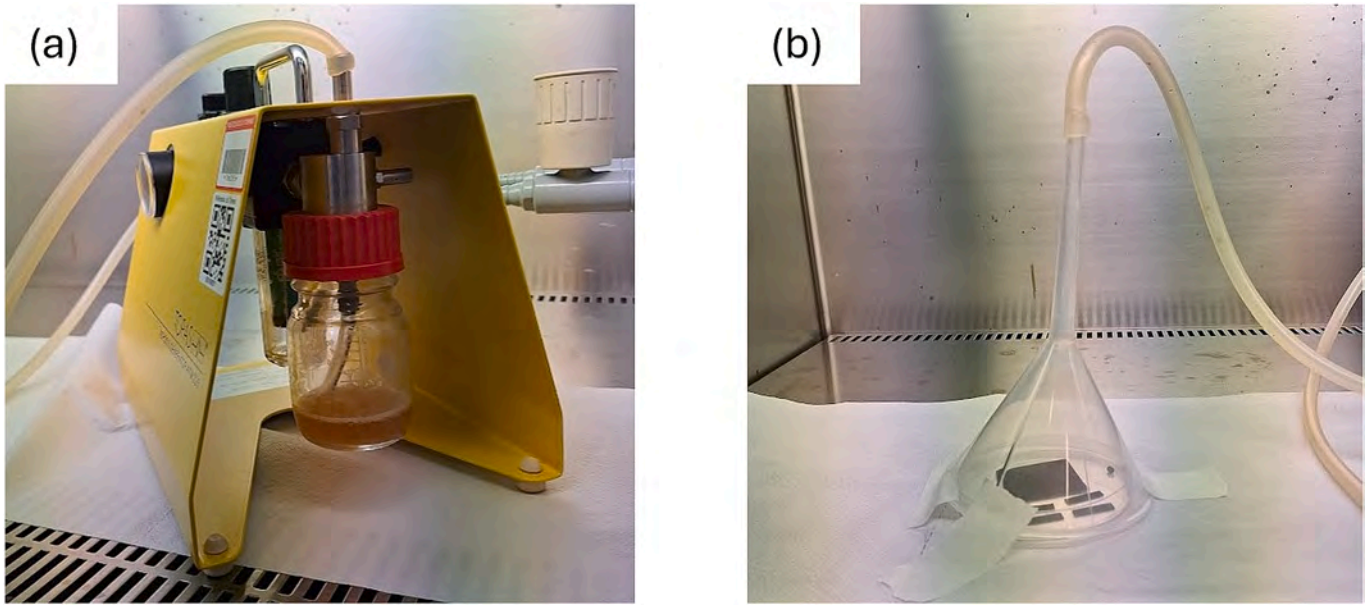

Fig. 1. Contamination test: (a) bioaerosol generation setup used for the contamination test, showing the bacterial suspension inside the generator; (b) arrangement of filter samples in a Petri dish, with a funnel placed on top to guide the bioaerosol flow directly onto the samples during exposure.

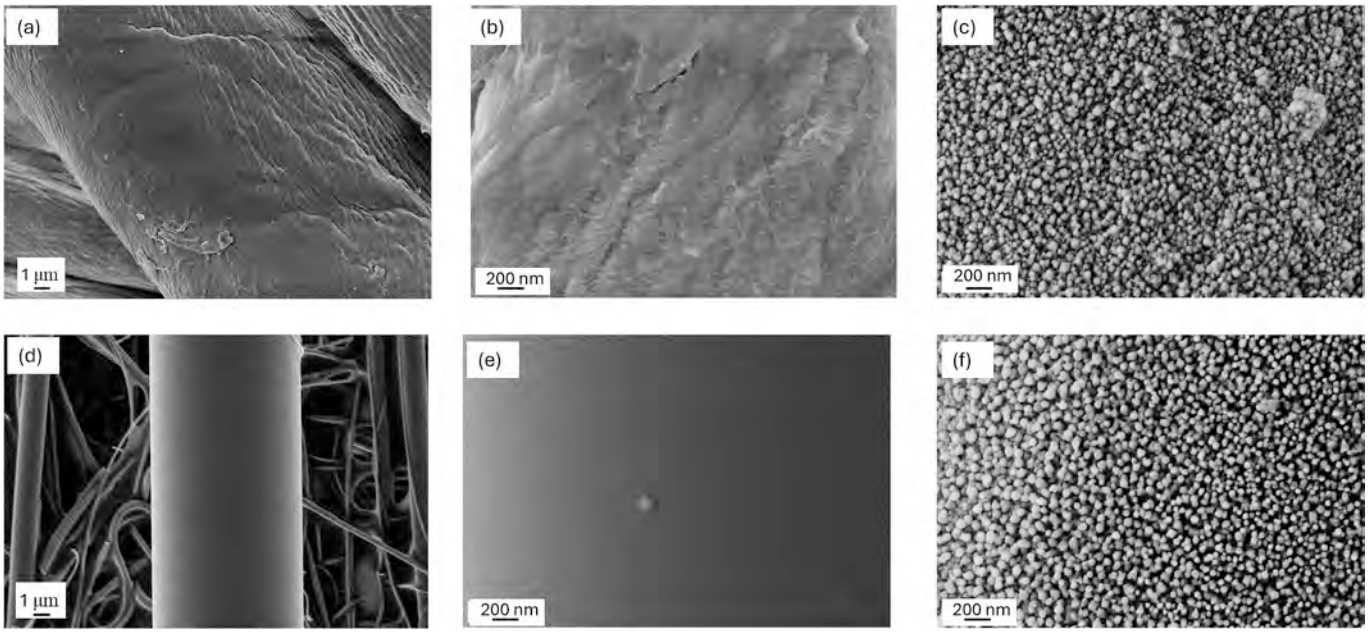

Fig. 2. FESEM images at low magnification of (a) uncoated cotton; (d) uncoated HEPA. FESEM images at high magnification of (b) uncoated cotton and (e) uncoated HEPA. FESEM images at high magnification of (c) SiO_2–ZrO_2–Ag coated cotton and (f) SiO_2–ZrO_2–Ag coated HEPA.

directly confirm the incorporation of silver nanoclusters within the SiO_2–ZrO_2 matrix, STEM and elemental mapping analyses were performed (Fig. 3). TEM observations suggested the presence of nanoscale Ag-rich domains embedded within the amorphous oxide matrix. In addition, Ag elemental mapping confirmed the homogeneous spatial distribution of silver throughout the coating. These observations provide strong evidence supporting the incorporation of Ag nanoclusters within the hybrid SiO_2–ZrO_2 structure.

However, the overall morphology appears similar to that previously obtained [14,17,35,39], despite the presence of a matrix deposited from two targets. Therefore, additional analyses were performed to confirm the presence of silver within the coating. EDS analyses corroborated the morphological observations, highlighting clear compositional differences between uncoated and coated substrates, as shown in Table 1. For the cotton fabrics, no detectable signals of Si, Zr, or Ag were found in the uncoated sample, confirming the absence of inorganic phases. In contrast, the SiO_2–ZrO_2 coating without silver nanoparticles exhibited silicon (5.13 at.%) and zirconium (1.57 at.%) content, indicating successful matrix deposition. In the SiO_2–ZrO_2–Ag coating, silver was additionally detected at 4.08 at.%, confirming the incorporation of Ag into the matrix. EDS measurements were performed at multiple areas on the sample surface to account for substrate heterogeneity. About the HEPA filter, EDS of the uncoated substrate revealed the silicon signal (~17.0 at.%) originating from the native material composed of glass fiber. In the coated HEPA filter, zirconium (1.27 at.%) and silver (1.71 at.%) were additionally detected, while the silicon content remained nearly constant, suggesting that the deposited layer contributed minimally to the overall Si signal. These findings confirm the effective incorporation of the SiO_2–ZrO_2–Ag coating, in agreement with previous reports on silica/silver and zirconia/silver coatings applied to glass-fiber and polymeric air filters [17,40].

EDS measurements were performed at multiple areas on the sample surface to account for substrate heterogeneity. The relatively higher standard deviation observed for Ag content in the cotton-based coating can be attributed to the intrinsic roughness and three-dimensional fibrous structure of the cotton substrate, which may locally influence coating thickness and consequently the detected Ag signal. Therefore, the observed variability is mainly associated with local morphological heterogeneity rather than with macroscopic inhomogeneity of the coating distribution.

To better understand the structural properties of the coatings, UV–Vis spectroscopy was performed and results for the SiO_2–ZrO_2 and SiO_2–ZrO_2–Ag coatings deposited on soda–lime glass model substrates are shown in Fig. 4(a). The SiO_2–ZrO_2 coating displayed a flat absorption profile across the visible spectrum, consistent with the negligible light absorption expected from a purely oxide matrix lacking plasmonic components. In contrast, the SiO_2–ZrO_2–Ag sample exhibited a distinct absorption band centred at 414 nm, corresponding to the localized surface plasmon resonance (LSPR) of Ag nanoclusters [41,42]. The presence and position of this band suggest the successful incorporation of Ag and the formation of nanoscale metallic clusters. The increased absorbance observed in the 500–800 nm region can be attributed to enhanced light scattering effects and to a broader size distribution and/or partial aggregation of Ag nanoclusters, which may lead to plasmon band broadening toward longer wavelengths [43].

XRD patterns of the SiO_2–ZrO_2 and SiO_2–ZrO_2–Ag coatings deposited on soda–lime glass model substrates are presented in Fig. 4(b). Both coatings exhibited a broad amorphous halo in the 2θ range of 20–35°, characteristic of non-crystalline silica/zirconia matrices. Although zirconia is typically crystalline, co-sputtering with silica suppresses its crystallization, leading to an amorphous phase. In the SiO_2–ZrO_2–Ag coating, the diffraction peaks located at approximately $2\theta \approx 38°$, 44°, 64°, and 77° were attributed to the (111), (200), (220), and (311) planes of face-centered cubic (fcc) metallic Ag, respectively, in agreement with standard reference data (JCPDS No. 04-0783) [44,45]. A rough estimation based on the Scherrer equation, using the Ag (111) reflection, suggested an average crystallite size of approximately 44 nm, confirming the nanoscale nature of the Ag crystalline domains. However, due to peak broadening, the absence of instrumental broadening correction, and the partially amorphous character of the SiO_2–ZrO_2 matrix, this value should be regarded only as an approximate indication. These findings support the coexistence of an amorphous oxide matrix and crystalline Ag nanoclusters, in agreement with previous studies on similar composite coatings [14,17,40].

Although XPS analysis would provide further insight into the oxidation state of silver and the chemical bonding within the SiO_2–ZrO_2 network, the combined evidence from XRD and UV–Vis analyses supports the presence of metallic Ag nanoclusters embedded in the oxide

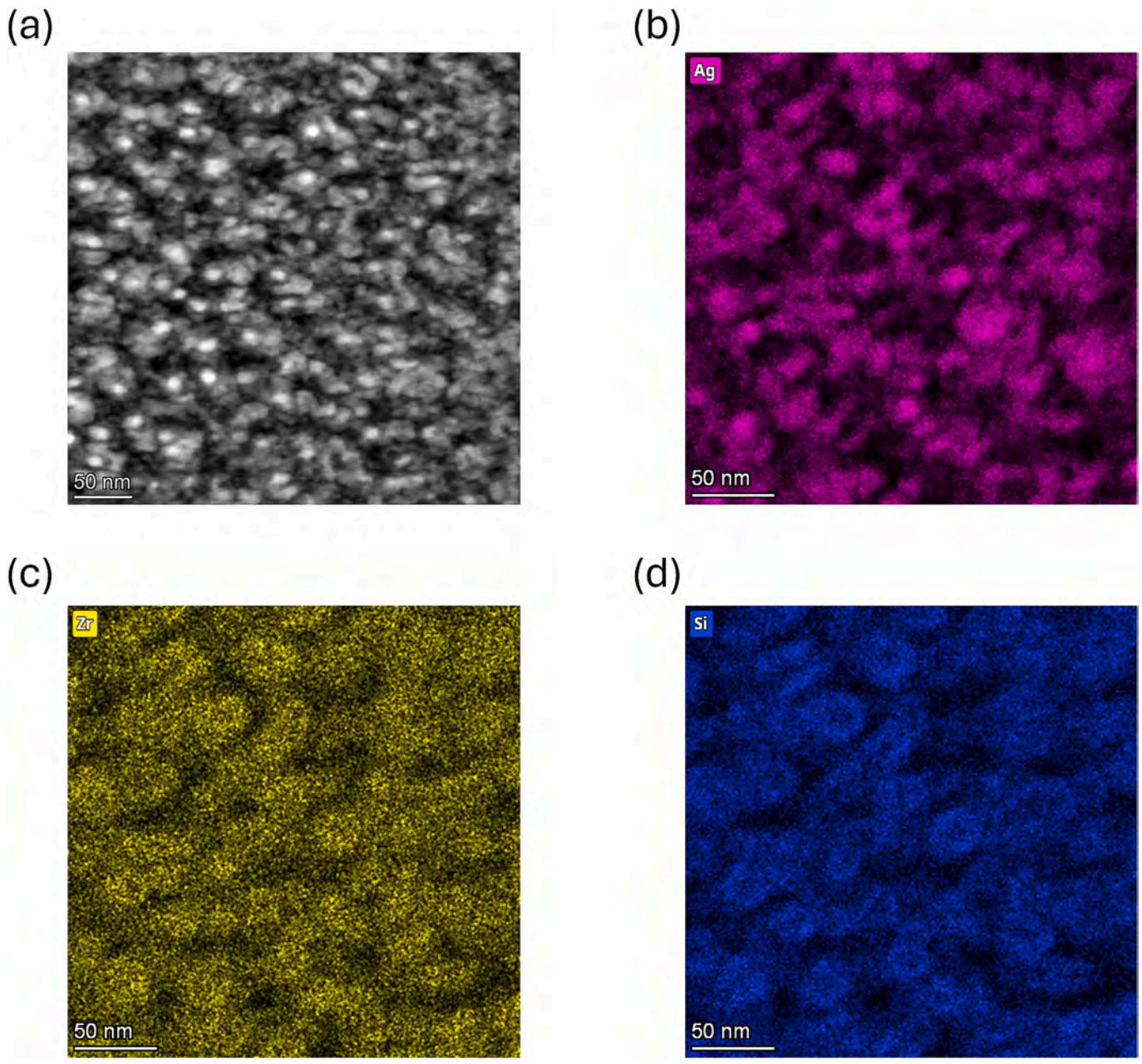

Fig. 3. STEM and STEM-EDS characterization of the SiO_2–ZrO_2–Ag coating. (a) TEM image showing the morphology of the matrix and Ag nanoclusters; (b–d) STEM-EDS elemental maps illustrating the distribution of Si, Zr, and Ag within the coating.

Table 1
Result of the EDS compositional analysis of Si, Zr and Ag content (in %at) in uncoated cotton and HEPA, on SiO_2-ZrO_2 coating and on SiO_2-ZrO2-Ag coating on cotton and HEPA.

	Si [% at.]	Zr [% at.]	Ag [% at.]
Uncoated COTTON	0.05 ± 0.05	n.d.	n.d
Uncoated HEPA	16.95 ± 0.67	n.d.	n.d.
SiO_2-ZrO_2	1.44 ± 0.15	1.39 ± 0.08	n.d.
COTTON_SiO_2-ZrO_2-Ag	2.47 ± 0.46	1.52 ± 0.18	4.08 ± 1.16
HEPA_SiO_2-ZrO_2-Ag	16.89 ± 1.00	1.27 ± 0.11	1.71 ± 0.15

n.d. = not detected.

matrix. In addition, the observed durability during washing tests and the controlled Ag^+ release behaviour suggest an effective stabilization of silver within the hybrid structure. Therefore, the present results provide indirect but consistent evidence of the functional role of the SiO_2–ZrO_2 matrix.

3.2. Silver ions release

The silver ion release kinetics were monitored over a 14-day immersion period in aqueous medium, as shown in Fig. 5. The Ag^+ concentration exhibited a rapid initial increase, reaching a peak at day 7 (~0.45 ppm) followed by a slight decline by day 14 (~0.4 ppm), indicating a sustained release behaviour. Notably, the release obtained from the silica–zirconia composite matrix exhibits intermediate performance between that of pure silica and pure zirconia matrices: in a previous study [17], the pure silica coating showed a higher Ag^+ release after 7 days, whereas the present composite system displays a more gradual profile that suggests the potential for prolonged antibacterial activity (as confirmed in Section 3.3). In addition, as already shown in [46], the

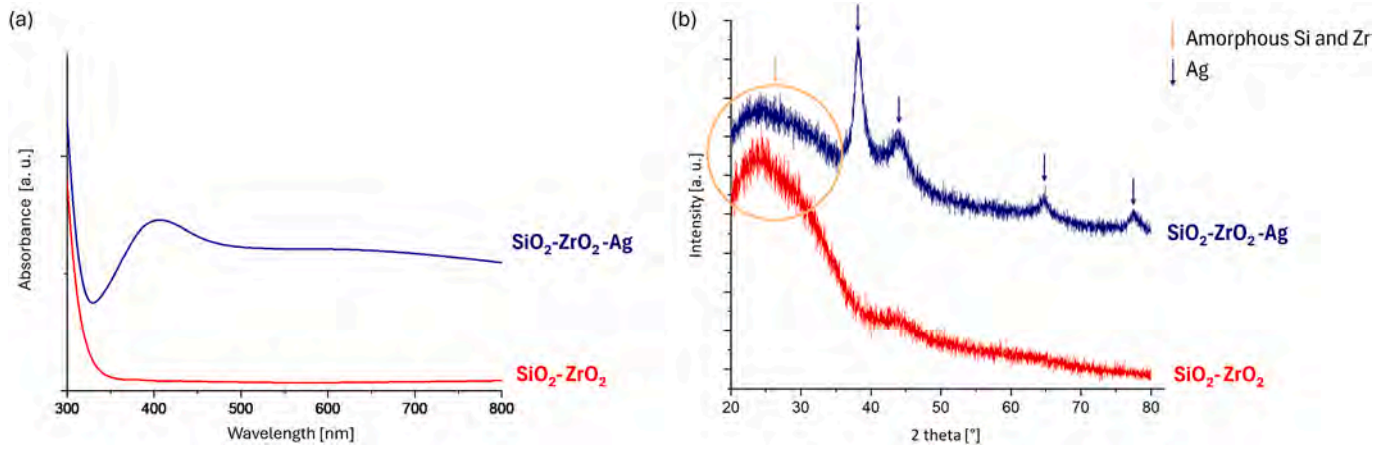

Fig. 4. Microstructural investigations: (a) UV–Vis analysis and (b) XRD on SiO_2–ZrO_2 and SiO_2–ZrO_2–Ag coatings deposited on soda-lime glass.

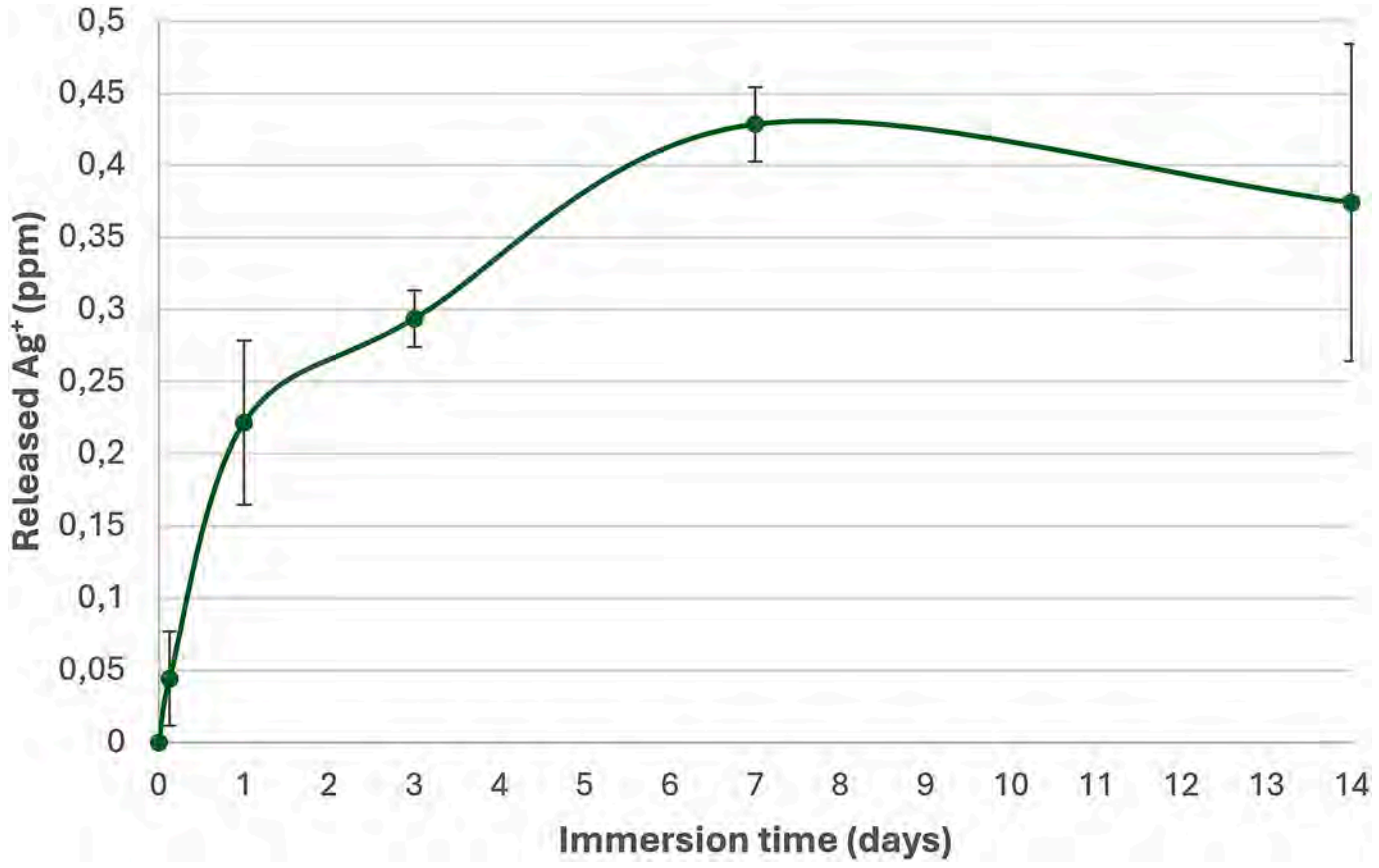

Fig. 5. Silver ion release profile (in water) of SiO_2–ZrO_2–Ag coating on cotton fabrics over 14 days.

presence of an Ag-embedding soluble matrix is crucial to improve control over silver ion release, if compared to systems based on AgNPs with no matrix support.

Such slow and sustained Ag release is crucial to balance effective antibacterial performance with biosafety in applications involving extended contact with biological environments.

3.3. Antibacterial tests

3.3.1. Inhibition halo test

The inhibition halo assay was conducted on both cotton and HEPA filter substrates to qualitatively confirm the antibacterial efficacy of the SiO_2–ZrO_2–Ag coating. The tests were performed against *Staphylococcus epidermidis* and *Escherichia coli* bacteria strains, evaluating the coated substrates and uncoated ones, the latter used as negative controls. The results of inhibition halo test on cotton and HEPA filters are reported in Fig. 6 (a) and (b), respectively.

After 24 h of incubation, no inhibition halos were observed around uncoated samples, but some colonies grew in contact with the samples, confirming the absence of any intrinsic antibacterial property in the base substrates. For both cotton and HEPA substrates, the antibacterial response of the SiO_2–ZrO_2–Ag coating was clearly strain-dependent. In the case of *S. epidermidis*, a well-defined and clear inhibition halo (dimension about 2 cm), completely free of bacterial colonies, was

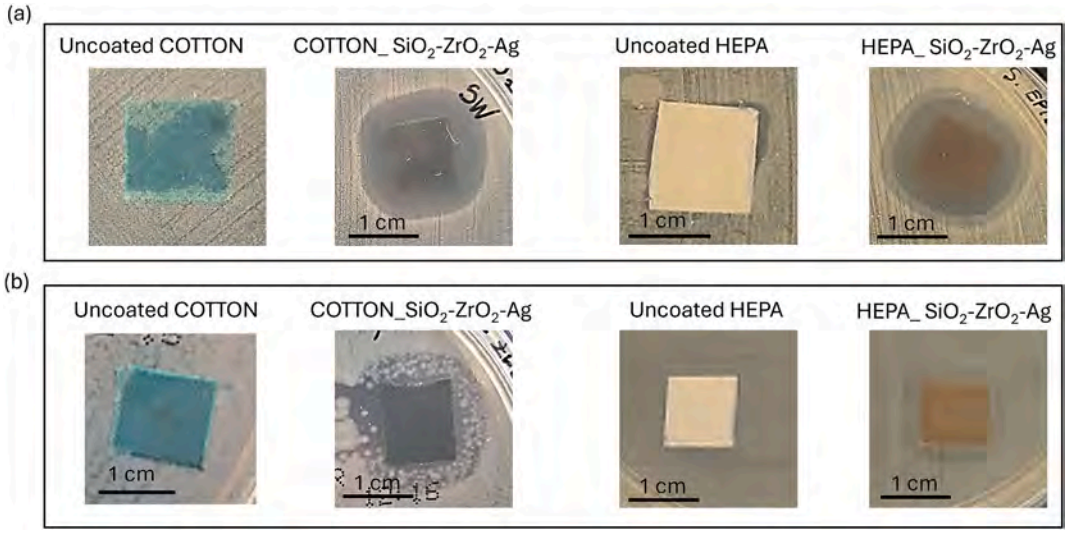

Fig. 6. Inhibition halo test against (a) *S. epidermidis* and (b) *E. coli* on Uncoated COTTON, COTTON_SiO_2_ZrO_2_Ag, uncoated HEPA and HEPA_SiO_2_ZrO_2_Ag.

consistently observed around both substrates, indicating an effective and localized bactericidal action. Notably, in the case of HEPA substrates, the well-defined primary inhibition halo was accompanied by the presence of an outer peripheral region characterized by reduced bacterial density, although not completely free of colonies. The observation of this additional peripheral region suggests a prolonged and spatially extended antimicrobial effect, as already described in other works [47,48]. Conversely, for *E. coli*, no sharply delineated "no-growth" inhibition halo was observed. In the case of coated cotton samples, a very narrow region immediately surrounding the sample appeared almost free of bacterial colonies. This inner region was followed by a broader area characterized by a reduced bacterial density compared to the background lawn, indicating partial growth suppression rather than complete inhibition.

In contrast, HEPA-based samples exhibited a more complex halo structure. In this case, a double halo could be observed around the coated samples: an inner region close to the sample where bacterial colonies were still present but with a relatively higher density, followed by a wider outer region where the bacterial growth appeared visibly reduced. This pattern suggests a spatially heterogeneous antibacterial effect.

Furthermore, a difference in the overall halo size was observed between the two substrates, which is likely related to the different structural and physicochemical properties of cotton and HEPA filters, potentially influencing the diffusion and local availability of antimicrobial species.

These findings are consistent with results reported in previous studies, which have also shown a more pronounced antibacterial effect against Gram-positive rather than Gram-negative bacteria [14]. The stronger inhibitory response observed here against *S. epidermidis* compared with *E. coli* is consistent with our previous findings. In a former study carried out by the same research group [40], a zirconia–silver nanocomposite coating was deposited using the same technique onto polymeric membranes for water filtration. In addition to inhibition halo measurements, that work also included filtration tests performed with suspensions containing both Gram-positive and Gram-negative bacteria. Under those conditions, the nanocomposite led to an almost complete reduction of *B. subtilis* and a substantial decrease in L. *monocytogenes*, whereas the antibacterial effect against *E. coli* remained only partial and did not achieve full inactivation. These outcomes further suggest that Ag-based coatings tend to exhibit higher effectiveness toward Gram-positive strains, likely due to differences in cell wall architecture and associated susceptibility. In support of this, zirconia filters containing silver nanoparticles were developed and demonstrated a strong effect against *S. aureus* but not against *E. coli* [49]. In addition, in [50], the Gram-positive *B. subtilis* strain was found to be more sensitive than *E. coli* to hybrid silica-hydroxypropylmethylcellulose, SiO_2–HPMC, materials containing silver nanoparticles, an effect attributed to structural differences in the bacterial cell wall and, consequently, to the distinct ability of silver nanoparticles to inhibit growth. Similarly, our observations are in agreement with the work of *Azocar* et al. [51] who reported stronger antibacterial activity of hybrid zirconia films with silver nanoparticle coatings, obtained by sol-gel method, against Gram-positive bacteria. In that study, larger inhibition zones were obtained for *S. aureus* and L. *monocytogenes* and this behaviour was mainly ascribed to the structure of the Gram-positive bacterial cell membrane. The thicker peptidoglycan layer and the presence of negatively charged teichoic acids may promote the interaction with Ag^+ ions and facilitate membrane permeabilization, whereas the additional outer membrane of Gram-negative bacteria may act as a diffusion barrier, limiting nanoparticle penetration and ion transport.

3.3.2. *Durability of antibacterial coatings under repeated washing*

Although conventional HEPA filtration media are generally not intended to be washed during practical use, accelerated aqueous exposure tests are widely employed to assess the chemical durability, coating adhesion, and retention of functional properties under harsh conditions. In the present work, washing experiments were not designed to reproduce real HEPA maintenance procedures, but rather to provide a severe stability assessment of the SiO_2–ZrO_2–Ag coating system under repeated aqueous stress. Although these conditions are intentionally more severe than real HEPA operating environments, they provide useful information regarding coating robustness under prolonged humidity exposure or accidental contact with moisture, conditions that may still occur in HVAC systems during service.

The washing durability study was carried out to evaluate coating stability and the persistence of antibacterial properties after repeated washings. For this test, cotton was used as model substrate, in order to simulate extreme aqueous exposure. Compositional analysis by EDS (Fig. 7) revealed a progressive decrease in the atomic percentages of Si, Zr, and Ag, indicating partial dissolution of the coating during repeated washing. In particular, the silver content decreased by ~50% after 5 cycles and remained relatively stable up to 20 cycles. This stabilization suggests that a fraction of Ag remained embedded in the SiO_2–ZrO_2 matrix, contributing to sustained antimicrobial functionality. The incorporation of Ag within the SiO_2–ZrO_2 network provides controlled release behaviour and improved coating retention. This observation is

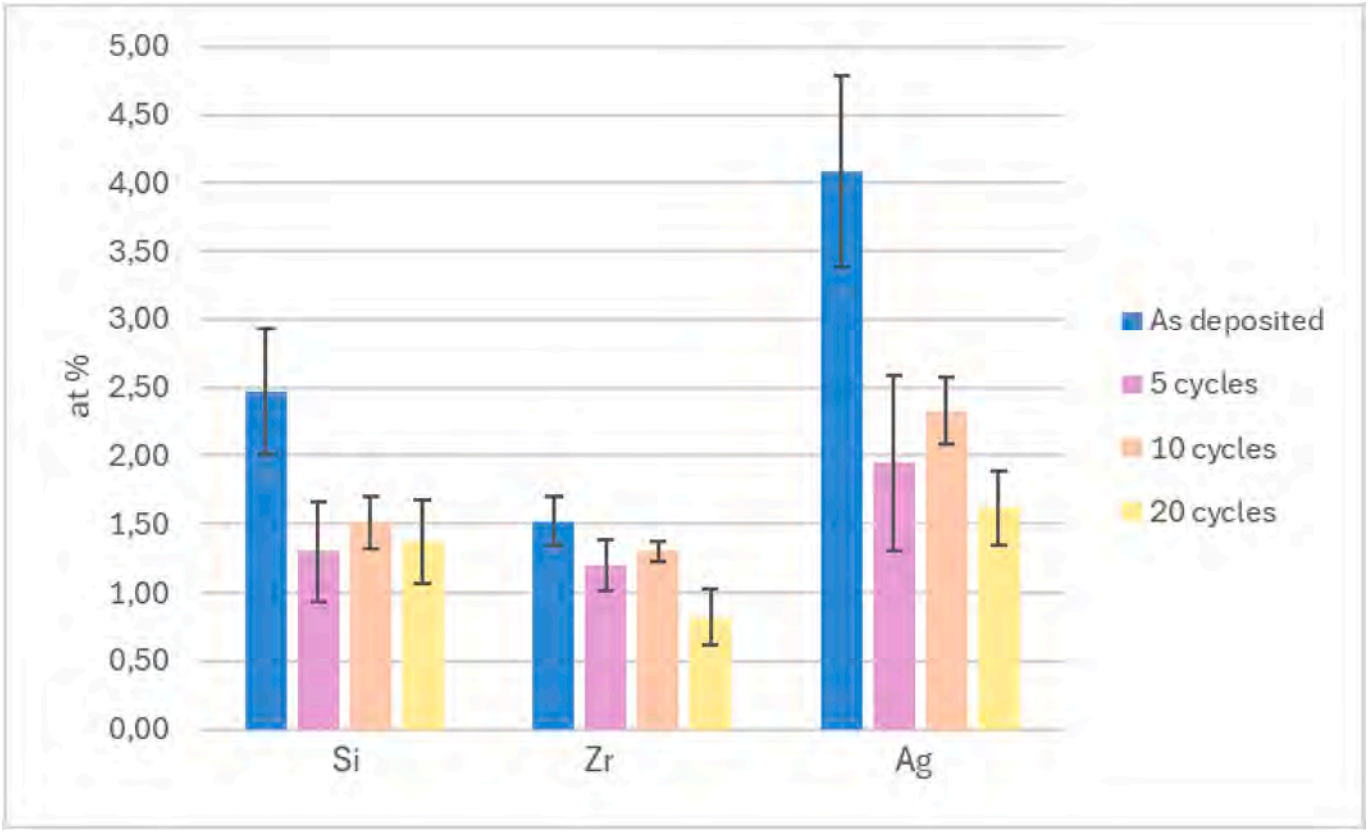

Fig. 7. Compositional analysis of SiO_2–ZrO_2–Ag coated cotton in the as-deposited form and after 5, 10 and 20 simulated washing cycles.

consistent with previous studies reporting that embedding silver nanoparticles within inorganic or hybrid matrices can reduce rapid silver depletion and enhance long-term stability by moderating Ag^+ release [52,53]. The silicon content decreased from about 2.47 at.% to 1.15 at.% after 5 cycles and then plateaued, reflecting the high solubility of the silica component. By contrast, the zirconium content remained nearly constant at ~0.90 at.%, demonstrating its superior resistance to aqueous environments. These findings are consistent with previous studies [17], which reported high solubility for silica-based coatings and enhanced stability for zirconia. Although absolute compositional values obtained by EDS should be interpreted cautiously due to the semi-quantitative nature of the technique, the observed compositional trends after washing were reproducible across multiple measurements. The reported standard deviations mainly reflect the intrinsic heterogeneity and rough

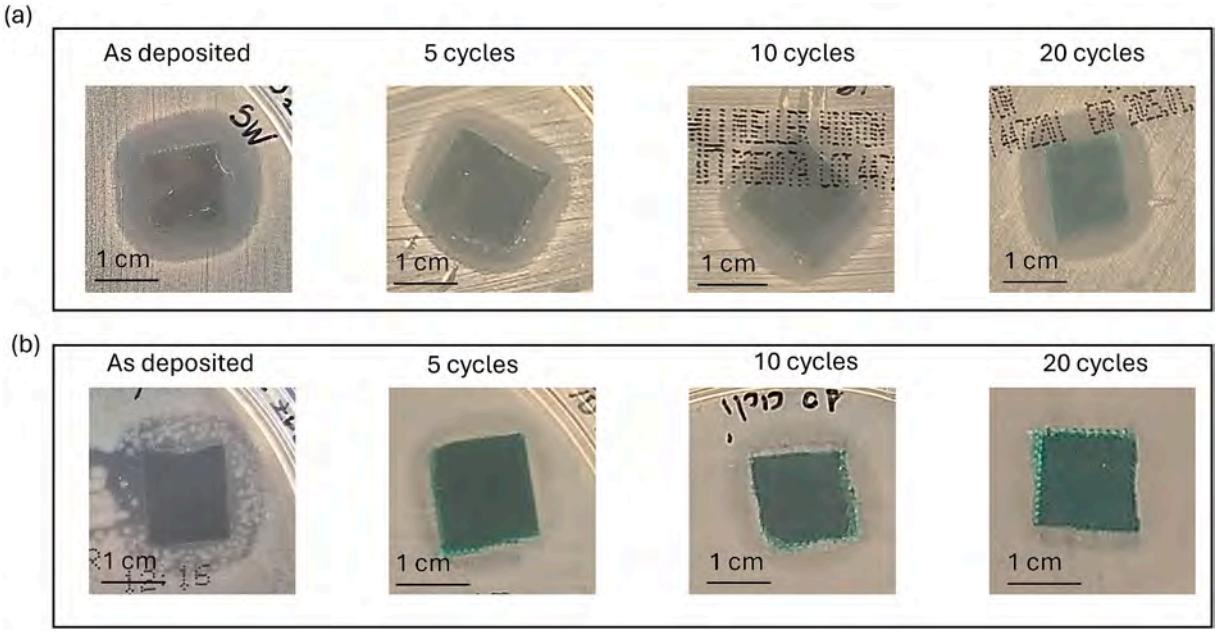

Fig. 8. Inhibition halo test against (a) *S. epidermidis* and (b) *E. coli* on COTTON_SiO_2_ZrO_2_Ag as deposited, and after 5, 10 and 20 simulated washing cycles.

fibrous morphology of the substrate. In this regard, it is also worth highlighting that zirconia is frequently employed in biomedical applications involving exposure to aqueous environments due to its remarkable resistance to dissolution. These results align with the main objective of the study, namely improving the water stability of silica-based coatings through zirconia incorporation, since silica alone is known to dissolve under aqueous exposure [17], in order to have a controlled and more prolonged release of silver ions. The observed stabilization of silver within the hybrid oxide network further highlights the advantage of the SiO_2–ZrO_2 matrix compared to pure silver coatings, which are often characterized by rapid ion release and limited long-term stability. By moderating Ag^+ release and improving coating durability, the hybrid structure may contribute to reducing excessive silver dispersion into the environment while maintaining prolonged antibacterial functionality.

Inhibition halo tests (Fig. 8) confirmed the persistence of antibacterial activity after repeated washing. For *S. epidermidis*, distinct inhibition zones were still detectable after 20 cycles, albeit with slightly reduced diameters (from about 2.0 cm to about 1.4 cm), in agreement with the partial Ag loss observed by EDS. Against *E. coli*, inhibition halos were less pronounced, showing only partial growth suppression: this outcome is in line with the previously described reduced susceptibility of Gram-negative bacteria. Overall, the SiO_2–ZrO_2–Ag coating exhibited good chemical durability and retained significant antibacterial performance after multiple washing cycles, supporting its potential for applications requiring long-term antimicrobial protection.

The washing-resistance tests clearly demonstrate that the SiO_2–ZrO_2–Ag coating, although undergoing partial dissolution during repeated aqueous exposure, still retains a significant antibacterial functionality. The rapid decrease in Si content after the first washing cycles is consistent with the well-known solubility of silica-based coatings in water, as also reported by previous studies on sputtered SiO_2–Ag systems [17]. In contrast, the ZrO_2 fraction remained remarkably stable, confirming its role as the chemically robust phase within the composite matrix [54]. This behaviour aligns with literature evidence showing that zirconia-containing coatings exhibit superior resistance to hydrolytic degradation and maintain structural integrity even under prolonged immersion in aqueous media [55].

The stabilization of silver within the composite matrix is further supported by the Ag release profile, which showed a slow and sustained ion release over 14 days. Similar trends have been reported for SiO_2–ZrO_2–Ag hybrid films [56] and for Ag-loaded ceramic membranes [57], where the oxide network effectively limits nanoparticle aggregation and prevents rapid leaching. The partial but not complete loss of Ag after washing cycles suggests that a fraction of the nanoclusters remains strongly embedded within the hybrid oxide matrix, ensuring continued antibacterial activity despite surface erosion.

Compared to the unwashed samples these results indicate that enough silver remains available to inhibit bacterial growth, in agreement with the stabilization of Ag within the composite matrix.

3.3.3. CFU counting test

For a more in-depth understanding, the antibacterial performance of the SiO_2–ZrO_2–Ag coating deposited on HEPA H14 filter was quantitatively evaluated against *S. epidermidis* (Fig. 9), using the CFU counting test. As explained, the bacterial proliferation in the broths containing the samples and on the surface of the filters (vortexed samples) was analysed.

The results for the broth analysis, shown in Fig. 9(a), demonstrated that the initial inoculum of 5×10^5 CFU/mL (red line in the figure) proliferated extensively in the broth-only control and in the presence of uncoated filters, reaching $\sim 10^{11}$ and $\sim 10^{14}$ CFU/mL, respectively. In contrast, broths containing the coated filters reached only $\sim 10^6$ CFU/mL, confirming strong inhibition of bacterial proliferation in the medium. Considering the proliferated colonies on sample surface, Fig. 9(b) showed significant differences in bacterial adhesion. On the uncoated filters, a quantity of about $\sim 10^8$ CFU/mL of bacterial colonies proliferated, whereas those from coated filters showed drastically reduced values of $\sim 10^4$ CFU/mL. These findings demonstrate not only the bactericidal effect of the coating in the surrounding medium but also its anti-adhesive action in limiting bacterial colonization of the filter surface.

3.3.4. Contamination test

In order to further investigate antibacterial performance under dynamic and realistic exposure scenarios, coated and uncoated HEPA H14 filters were challenged with a concentrated bacterial aerosol of *S. epidermidis*.

Qualitative evaluation (Fig. 10) revealed complete inhibition of bacterial growth on coated filters, while uncoated samples showed extensive colony formation. This confirms the ability of the Ag-containing coating to suppress airborne bacterial contamination deposited on the filter surface.

For the quantitative assessment, filters were immersed in sterile broth after contamination and incubated for 24 h. Subsequent CFU counts (Fig. 11) confirmed that bacterial counts reached $\sim 10^{13}$ CFU/mL in broths incubated with uncoated filters, whereas coated filters limited the bacterial growth to $\sim 10^1$ CFU/mL. Similar differences were observed in the vortexed suspensions, which provided assessment of the bacteria adhered to the filter surface: uncoated filters released up to $\sim 10^8$ CFU/mL, while the coated ones released only $\sim 10^2$ CFU/mL.

Overall, these results demonstrate that the SiO_2–ZrO_2–Ag coating

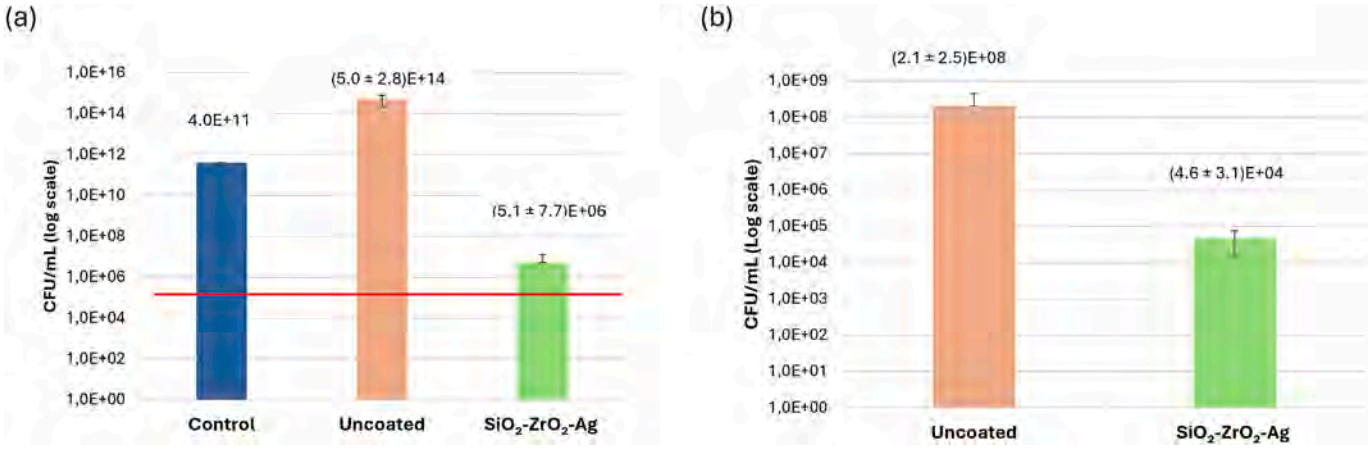

Fig. 9. Quantification of proliferated *Staphylococcus epidermidis* on HEPA H14 filters: (a) bacterial proliferation in broth after contact with uncoated and SiO_2–ZrO_2–Ag–coated filters (the red line indicates the initial bacterial load); (b) bacterial adhesion on uncoated and coated filters after incubation.

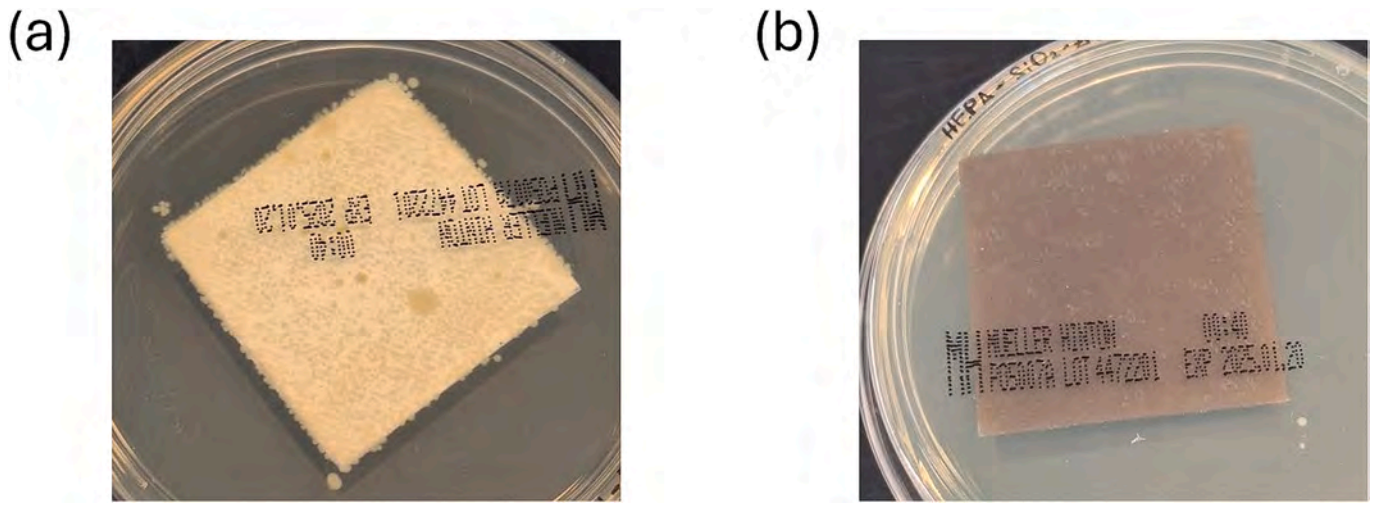

Fig. 10. Qualitative evaluation of *Staphylococcus epidermidis* proliferation on HEPA H14 filters after contamination using a bioaerosol generator: (a) bacterial proliferation on an uncoated HEPA H14 filter, and (b) bacterial proliferation on SiO_2-ZrO_2-Ag coated HEPA H14.

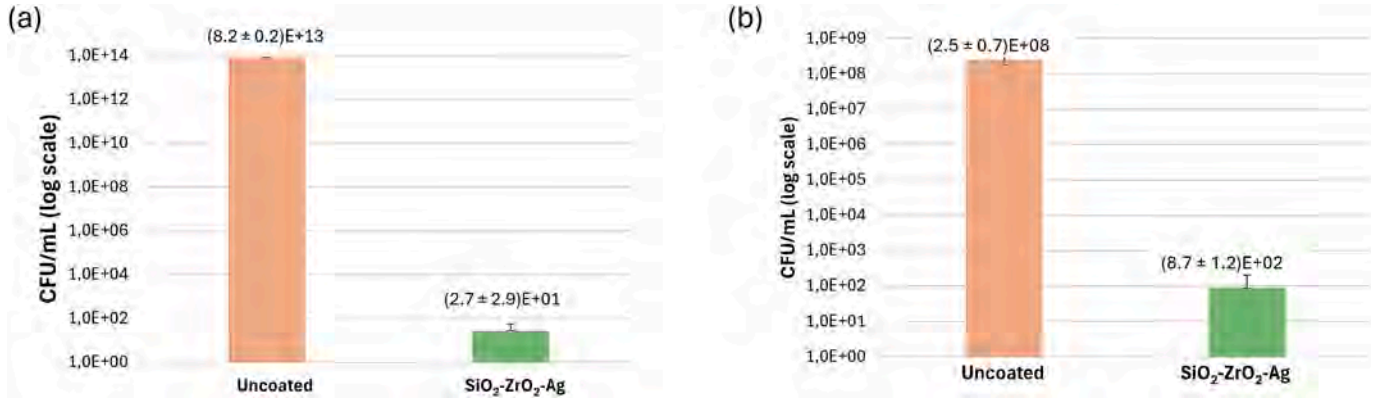

Fig. 11. Quantification of proliferated *Staphylococcus epidermidis* on HEPA H14 filters after contamination using a bioaerosol generator: (a) bacterial proliferation in broth after contact with contaminated uncoated and SiO_2–ZrO_2–Ag–coated filters, (b) bacterial adhesion on contaminated uncoated and coated filters after incubation.

effectively prevents both airborne bacterial contamination and filter colonization. This dual activity, i.e. suppression of bacterial proliferation in the surrounding medium and inhibition of surface adhesion, highlights the coating suitability for applications requiring reliable microbial control under realistic operational conditions.

The bioaerosol contamination test provides a realistic assessment of the coating performance under conditions mimicking actual HVAC operation. The coated filters showed a drastic reduction in viable bacteria both on the surface and in the broth after exposure, confirming that the antimicrobial layer remains effective even when challenged with airborne microorganisms. This is particularly relevant because bioaerosol deposition typically leads to rapid colonization of filter fibers, promoting re-aerosolization and secondary contamination.

4. Conclusions

In this work, we developed SiO_2–ZrO_2–Ag composite coatings via PVD co-sputtering on cotton fabrics and HEPA H14 filters and provided a comprehensive structural and functional characterization. Coatings exhibited stronger activity against Gram-positive *Staphylococcus epidermidis*, while maintaining measurable effects on Gram-negative *Escherichia coli*. Durability tests showed that the coatings preserve a significant antibacterial performance after repeated washing cycles, with zirconia contributing to matrix stability and enabling sustained silver release. The SiO_2–ZrO_2–Ag coatings represent a promising and potentially scalable approach for antimicrobial textiles and filtration systems. Their combination of chemical stability, controlled ion release, and broad-spectrum efficacy provides a solid basis for the development of next-generation antimicrobial surfaces for healthcare and air-quality applications.

CRediT authorship contribution statement

Angelica Luceri: Writing – review & editing, Writing – original draft, Visualization, Methodology, Formal analysis, Data curation. **Mariacristina Martorino:** Writing – review & editing, Methodology. **Francesco Baino:** Writing – review & editing, Supervision, Project administration, Funding acquisition. **Cristina Balagna:** Writing – review & editing, Supervision, Formal analysis, Conceptualization.

Declaration of competing interest

The authors declare that they have no known competing financial interests or personal relationships that could have appeared to influence the work reported in this paper.

Acknowledgments

This research work was performed within the framework of a project funded under the National Recovery and Resilience Plan (NRRP), Mission 4 Component 2 Investment 1.3—Call for tender No. 1561 of 11.10.2022 of Ministero dell'Università e della Ricerca (MUR); the project was funded by the European Union—NextGenerationEU. Project details: project code PE0000021, Concession Decree No. 1561 of 11.10.2022 adopted by Ministero dell'Università e della Ricerca (MUR), CUP E13C22001890001, Project title "Network 4 Energy Sustainable Transition—NEST".

Francesco Romano from Politecnico di Milano is kindly acknowledged for providing the HEPA H14 substrates to be sputtered.

Data availability

Data will be made available on request.

References

[1] S. Wallbanks, B. Griffiths, M. Thomas, O.J. Price, K.P. Sylvester, Impact of environmental air pollution on respiratory health and function, Physiol. Rep. 12 (2024) e70006, https://doi.org/10.14814/phy2.70006.
[2] T.Z. Maung, J.E. Bishop, E. Holt, A.M. Turner, C. Pfrang, Indoor air pollution and the health of vulnerable groups: a systematic review focused on particulate matter (PM), volatile organic compounds (VOCs) and their effects on children and people with pre-existing lung disease, Int. J. Environ. Res. Public Health 19 (2022) 8752, https://doi.org/10.3390/ijerph19148752.
[3] O.P. Bansal, A review of the indoor air quality of hospitals and healthcare centres, Int. J. Biol. Pharm. Sci. Arch. 8 (2024) 113–127, https://doi.org/10.53771/ijbpsa.2024.8.1.0076.
[4] A. Loureiro, A. Ferreira, N. Barros, Systematic review of the literature on indoor air quality in healthcare units and its effects on health, BMC Public Health 25 (2025) 2398, https://doi.org/10.1186/s12889-025-23445-1.
[5] N. Ayuba, G.H. Justi, G.C. Lopes, Numerical study of cough droplets dispersion in indoor and quiescent environment: influence of droplet size and air humidity, Rev. Principia 62 (2025), https://doi.org/10.18265/2447-9187a2025id8833.
[6] D. Obitková, M. Mráz, E. Pavlík, Virus removal by high-efficiency air (HEPA) filters and filtration capacity enhancement by nanotextiles: a pilot study, Folia Microbiol. (Praha) 69 (2024) 459–464, https://doi.org/10.1007/s12223-024-01137-4.
[7] H. Ting Wu, Q. Shuang Li, R. Chen Dai, S. Liu, L. Wu, W. Mao, C. Hua Ji, Effects of air-conditioning systems in the public areas of hospitals: a scoping review, Epidemiol. Infect. 149 (2021) e20, https://doi.org/10.1017/S0950268821001990.
[8] H. Salonen, T. Salthammer, E. Castagnoli, M. Täubel, L. Morawska, Cleaning products: their chemistry, effects on indoor air quality, and implications for human health, Environ. Int. 190 (2024) 108836, https://doi.org/10.1016/j.envint.2024.108836.
[9] G. Zheng, G.M. Filippelli, A. Salamova, Increased indoor exposure to commonly used disinfectants during the COVID-19 pandemic, Environ. Sci. Technol. Lett. 7 (2020) 760–765, https://doi.org/10.1021/acs.estlett.0c00587.
[10] A.R. Urrutia, S.P. Stawicki, C.N. Kimble, K.C. Worrilow, The clinical and environmental effects of an advanced air purification technology in multiple healthcare settings, Sci. Technol. Built Environ. 29 (2023) 858–870, https://doi.org/10.1080/23744731.2023.2266349.
[11] S.P. Stawicki, A.R. Urrutia, C.N. Kimble, K.C. Worrilow, Proven impact of an advanced air purification system in the reduction of infectious airborne and surface pathogens, concomitant reduction of hospital-acquired infections and length of stay, and improvement in health-care economics, J. Global Infect. Dis. 15 (2023) 3–5, https://doi.org/10.4103/jgid.jgid_11_23.
[12] H. Alhussain, S. Ghani, N.O. Eltai, Breathing clean air: navigating indoor air purification techniques and finding the ideal solution, Int. J. Environ. Res. Public Health 21 (2024) 1107, https://doi.org/10.3390/ijerph21081107.
[13] H. Yazdani-Ahmadabadi, et al., Durable surfaces from film-forming silver assemblies for long-term zero bacterial adhesion without toxicity, ACS Cent. Sci. 8 (2022) 546–561, https://doi.org/10.1021/acscentsci.1c01556.
[14] A. Luceri, R. Francese, S. Perero, D. Lembo, M. Ferraris, C. Balagna, Antibacterial and antiviral activities of silver nanocluster/silica composite coatings deposited onto air filters, ACS Appl. Mater. Interfaces 16 (2024) 3955–3965, https://doi.org/10.1021/acsami.3c13843.
[15] X. Wang, W. Sun, W. Yang, S. Gao, C. Sun, Q. Li, Mesoporous silica-protected silver nanoparticle disinfectant with controlled Ag+ ion release, efficient magnetic separation, and effective antibacterial activity, Nanoscale Adv. 1 (2019) 840–848, https://doi.org/10.1039/C8NA00275D.
[16] S.Banu. A, J.Lakshmi. S. S., L. K.V., K. Mani Rahulan, Kaviyarasan S., Harnessing silica-coated silver nanoparticles for combating multidrug-resistant Pseudomonas aeruginosa, Appl. Microbiol. Biotechnol. 110 (2026) 14, https://doi.org/10.1007/s00253-025-13699-5.
[17] A. Luceri, S. Perero, A. Cochis, A. Scalia, L. Rimondini, M. Ferraris, C. Balagna, Washing resistant antibacterial composite coatings on cotton textiles, Cellulose 30 (2023) 9877–9897, https://doi.org/10.1007/s10570-023-05471-7.
[18] C. Balagna, S. Perero, F. Bosco, C. Mollea, M. Irfan, M. Ferraris, Antipathogen nanostructured coating for air filters, Appl. Surf. Sci. 508 (2020) 145283, https://doi.org/10.1016/j.apsusc.2020.145283.
[19] C. Balagna, M. Irfan, S. Perero, M. Miola, G. Maina, D. Santella, A. Simone, Characterization of antibacterial silver nanocluster/silica composite coating on high performance Kevlar® textile, Surf. Coat. Technol. 321 (2017) 438–447, https://doi.org/10.1016/j.surfcoat.2017.05.009.
[20] M. Laskowska, P. Kowalczyk, A. Karczmarska, K. Kramkowski, K. Wrzosek, Ł. Laskowski, A novel biocidal nanocomposite: spherical silica with silver ions anchored at the surface, Int. J. Mol. Sci. 24 (2023), https://doi.org/10.3390/ijms24010545.
[21] C. Fernández-Lodeiro, et al., Adenosine-monophosphate-assisted homogeneous silica coating of silver nanoparticles in high yield, Nanomaterials 13 (2023), https://doi.org/10.3390/nano13202788.
[22] S. Nuti, A. Fernández-Lodeiro, J. Galhano, E. Oliveira, M.P. Duarte, J.L. Capelo-Martínez, C. Lodeiro, J. Fernández-Lodeiro, Tailoring mesoporous silica-coated silver nanoparticles and polyurethane-doped films for enhanced antimicrobial applications, Nanomaterials 14 (2024) 5, https://doi.org/10.3390/nano14050462.
[23] M. Hidayat, A. Adlim, I. Maulana, M. Zulfajri, Immobilization of silver nanoparticles on chitosan-coated silica-gel-beads and the antibacterial activity, Key Eng. Mater. 892 (2021) 36–42, https://doi.org/10.4028/www.scientific.net/KEM.892.36.
[24] M. Arkas, et al., Hybrid silica xerogel and titania/silica xerogel dispersions reinforcing hydrophilicity and antimicrobial resistance of leathers, Gels 9 (9) (Sep. 2023) 9, https://doi.org/10.3390/gels9090685.
[25] T.T. Trung, T.D. Loc, N.T. Si, N.T. Cong, V.V. Lenh, P.-T. Do, P.T.N. Nguyen, K. Q. Vo, Eco-friendly synthesis of silver nanoparticles from camellia Chrysantha (Hu) Tuyama with potential anti-COVID application: exploration via computational and experimental methods, Inorg. Chem. Commun. (2026) 116196, https://doi.org/10.1016/j.inoche.2026.116196.
[26] T.T. Trung, N.T.T. Huong, T.D. Loc, N.T. Si, V.Q. Khuong, P.T.N. Nguyen, Biogenic one-step synthesis of silver nanoparticles using Quisqualis indica Linn flower extract: characterization, molecular docking, and DFT studies, Inorg. Chem. Commun. 158 (2023) 111469, https://doi.org/10.1016/j.inoche.2023.111469.
[27] M. Peng, J.-L. Chuan, G. Zhao, Q. Fu, Construction of silver-coated high translucent zirconia implanting abutment material and its property of antibacterial, Artif. Cells Nanomed. Biotechnol. 51 (2023) 441–452, https://doi.org/10.1080/21691401.2023.2244013.
[28] H. Li, Z. Wang, H. Zhang, Z. Pan, Nanoporous PLA/(chitosan nanoparticle) composite fibrous membranes with excellent air filtration and antibacterial performance, Polymers 10 (2018) 1085, https://doi.org/10.3390/polym10101085.
[29] A. Ciorîță, M. Suciu, M. Coroș, C. Varodi, F. Pogăcean, L. Măgeruşan, V. Mirel, R.-I. Ștefan-van Staden, S. Pruneanu, Antibacterial enhancement of high-efficiency particulate air filters modified with graphene–silver hybrid material, Microorganisms 11 (2023) 745, https://doi.org/10.3390/microorganisms11030745.
[30] R. Watson, et al., Efficacy of antimicrobial and anti-viral coated air filters to prevent the spread of airborne pathogens, Sci. Rep. 12 (2022) 2803, https://doi.org/10.1038/s41598-022-06579-9.
[31] M. Blanco, C. Monteserín, E. Gómez, E. Aranzabe, J.L. Vilas Vilela, A. Pérez-Márquez, J. Maudes, C. Vaquero, N. Murillo, I. Zalakain, L. Ruiz Rubio, Polycarbonate nanofiber filters with enhanced efficiency and antibacterial performance, Polymers 17 (2025) 444, https://doi.org/10.3390/polym17040444.
[32] Y.H. Joe, W. Ju, J.H. An, J. Hwang, A quantitative determination of the antibacterial efficiency of fibrous air filters based on the disc diffusion method, Aerosol Air Qual. Res. 14 (2014) 928–933, https://doi.org/10.4209/aaqr.2013.04.0116.
[33] I. Nag, Development of a combinatory filtration system for pollution and virus abatement by optimized nanoparticle deposition, PLoS One 17 (2022) e0264991, https://doi.org/10.1371/journal.pone.0264991.
[34] M. Ferraris, C. Balagna, S. Perero, Method for the Application of an Antiviral Coating to a Substrate and Relative Coating, WO2019082001, 2019.
[35] M. Irfan, S. Perero, M. Miola, et al., Antimicrobial functionalization of cotton fabric with silver nanoclusters/silica composite coating via RF co-sputtering technique, Cellulose 24 (2017) 2331–2345, https://doi.org/10.1007/s10570-017-1232-y.
[36] NCCLS M2-A9, Performance Standards for Antimicrobial Disk Susceptibility Tests, Approved Standard, 9th ed., NCCLS, Villanova, PA, 2003.
[37] NCCLS (Ed.), Methods for Dilution Antimicrobial Susceptibility Tests for Bacteria That Grow Aerobically, Approved Standard 6th ed, NCCLS, Villanova, PA, USA, 2003. M7-A6,.
[38] CEN, CWA 18309:2025, Procedure for Testing the Antibacterial Effect of the Air Filter After Contamination Through a Bacterial Bioaerosol, European Committee for Standardization, Brussels, Belgium, 2025.
[39] C. Balagna, R. Francese, S. Perero, D. Lembo, M. Ferraris, Nanostructured composite coating endowed with antiviral activity against human respiratory viruses deposited on fibre-based air filters, Surf. Coat. Technol. 409 (2021) 126873, https://doi.org/10.1016/j.surfcoat.2021.126873.
[40] A. Luceri, M. Toppan, A. Calogero, A. Rinaldi, C. Balagna, Antibacterial nanocomposite ceramic coating for liquid filtration application, Nanomaterials 15 (2025) 911, https://doi.org/10.3390/nano15120911.
[41] M. Mulu, M. Tefera, A. Guadie, K. Basavaiah, Biosynthesis, characterization and study of the application of silver nanoparticle for 4-nitrophenol reduction, and antimicrobial activities, Biotechnol. Rep. 42 (2024) e00838, https://doi.org/10.1016/j.btre.2024.e00838.

[42] R. Dhir, S. Chauhan, P. Subham, S. Kumar, P. Sharma, A. Shidiki, G. Kumar, Plant-mediated synthesis of silver nanoparticles: unlocking their pharmacological potential—a comprehensive review, Front. Bioeng. Biotechnol. 11 (2024) 1324805, https://doi.org/10.3389/fbioe.2023.1324805.
[43] K.L. Kelly, E. Coronado, L.L. Zhao, G.C. Schatz, The optical properties of metal nanoparticles: the influence of size, shape, and dielectric environment, J. Phys. Chem. B 107 (3) (Jan. 2003) 668–677, https://doi.org/10.1021/jp026731y.
[44] Md.H. Ali, Md.A.K. Azad, K.A. Khan, Md.O. Rahman, U. Chakma, A. Kumer, Analysis of crystallographic structures and properties of silver nanoparticles synthesized using PKL extract and nanoscale characterization techniques, ACS Omega 8 (2023) 28133–28142, https://doi.org/10.1021/acsomega.3c01261.
[45] F. Koohpeima, M. Mokhtari, K. Samaneh, The effect of silver nanoparticles on composite shear bond strength to dentin with different adhesion protocols, J. Appl. Oral Sci. 25 (2017) 367–373, https://doi.org/10.1590/1678-7757-2016-0391.
[46] F. Gattucci, M. Rossi, L. Sarchini, C. Bertarelli, R. Castagna, C. Balagna, Silver-functionalized polyvinyl alcohol nanofiber membranes: a comparative study of nanoparticle incorporation and coating deposition, Surf. Coat. Technol. 520 (2026) 133038, https://doi.org/10.1016/j.surfcoat.2025.133038.
[47] C.P. Scott, P.A. Higham, Antibiotic bone cement for the treatment of *Pseudomonas aeruginosa* in joint arthroplasty: comparison of tobramycin and gentamicin-loaded cements, J. Biomed. Mater. Res. B Appl. Biomater. 64 (2003) 94–98, https://doi.org/10.1002/jbm.b.10515.
[48] C. Mollea, F. Bosco, D. Fissore, Agar plate methods for assessing the antibacterial activity of thyme and oregano essential oils against *S. epidermidis* and *E. coli*, Antibiotics 11 (12) (2022), https://doi.org/10.3390/antibiotics11121809.
[49] E. Rodrigues, E.J.P. Miranda Jr., M. Oliveira, Silver-doped zirconia nanoparticles as possible bactericide in water filters, Mater. Sci. Forum 798–799 (2014) 69–74, https://doi.org/10.4028/www.scientific.net/MSF.798-799.69.
[50] T. Angelova, N. Rangelova, H. Dineva, N. Georgieva, R. Müller, Synthesis, characterization and antibacterial assessment of SiO2-hydroxypropylmethyl cellulose hybrid materials with embedded silver nanoparticles, Biotechnol. Biotechnol. Equip. 28 (2014) 747–752, https://doi.org/10.1080/13102818.2014.944789.
[51] I. Azócar, E. Vargas, N. Duran, A. Arrieta, E. González, J. Pavez, M.J. Kogan, J. H. Zagal, M.A. Paez, Preparation and antibacterial properties of hybrid-zirconia films with silver nanoparticles, Mater. Chem. Phys. 137 (2012) 396–403, https://doi.org/10.1016/j.matchemphys.2012.09.042.
[52] M. Harun-Ur-Rashid, T. Foyez, S.B. Naidu Krishna, S. Poda, A. Bin Imran, Recent advances of silver nanoparticle-based polymer nanocomposites for biomedical applications, RSC Adv. 15 (11) (2025) 8480–8505. https://doi.org/10.1039/D4RA08220F.
[53] E. Dube, G.E. Okuthe, Silver nanoparticle-based antimicrobial coatings: sustainable strategies for microbial contamination control, Microbiol. Res. 16 (6) (Jun. 2025) 110, https://doi.org/10.3390/microbiolres16060110.
[54] K.L. Arun, M. Udhayakumar, N. Radhika, A comprehensive review on various ceramic nanomaterial coatings over metallic substrates: applications, challenges and future trends, J. Bio- Tribo-Corros. 9 (2022) 11, https://doi.org/10.1007/s40735-022-00717-6.
[55] B. Masheder, C. Urata, A. Hozumi, Transparent and hard zirconia-based hybrid coatings with excellent dynamic/thermoresponsive oleophobicity, thermal durability, and hydrolytic stability, ACS Appl. Mater. Interfaces 5 (2013) 7899–7905, https://doi.org/10.1021/am401992h.
[56] Y. Mei, J. Yang, R. Zhang, H. Li, Y. Guo, Enhanced antibacterial activity, dye rejection and anti-fouling performance of ZrO2-SiO2 composite ceramic membranes embedded by silver nanoparticles, J. Sol-Gel Sci. Technol. 114 (2025) 413–429, https://doi.org/10.1007/s10971-025-06697-6.
[57] S. Manna, M.K. Naskar, D. Saha, P. Pal, S.K. Medda, Long-term stability of Ag NPs in a room temperature cured SiO2–ZrO2 crosslinking hybrid robust coating towards enhanced weather resistance properties and its antibacterial applications, New J. Chem. 49 (2025) 6914–6929, https://doi.org/10.1039/D5NJ00611B.